© 2016. Published by The Company of Biologists Ltd | Journal of Experimental Biology (2016) 219, 392-403 doi:10.1242/jeb.129254

RESEARCH ARTICLE

Volumetric flow imaging reveals the importance of vortex ring formation in squid swimming tail-first and arms-first

Ian K. Bartol[1,*], Paul S. Krueger[2], Rachel A. Jastrebsky[1], Sheila Williams[2] and Joseph T. Thompson[3]

ABSTRACT

Squids use a pulsed jet and fin movements to swim both arms-first (forward) and tail-first (backward). Given the complexity of the squid multi-propulsor system, 3D velocimetry techniques are required for the comprehensive study of wake dynamics. Defocusing digital particle tracking velocimetry, a volumetric velocimetry technique, and high-speed videography were used to study arms-first and tail-first swimming of brief squid *Lolliguncula brevis* over a broad range of speeds [0–10 dorsal mantle lengths (DML) s^{-1}] in a swim tunnel. Although there was considerable complexity in the wakes of these multi-propulsor swimmers, 3D vortex rings and their derivatives were prominent reoccurring features during both tail-first and arms-first swimming, with the greatest jet and fin flow complexity occurring at intermediate speeds (1.5–3.0 DML s^{-1}). The jet generally produced the majority of thrust during rectilinear swimming, increasing in relative importance with speed, and the fins provided no thrust at speeds >4.5 DML s^{-1}. For both swimming orientations, the fins sometimes acted as stabilizers, producing negative thrust (drag), and consistently provided lift at low/intermediate speeds (<2.0 DML s^{-1}) to counteract negative buoyancy. Propulsive efficiency (η) increased with speed irrespective of swimming orientation, and η for swimming sequences with clear isolated jet vortex rings was significantly greater (η=78.6±7.6%, mean±s.d.) than that for swimming sequences with clear elongated regions of concentrated jet vorticity (η=67.9±19.2%). This study reveals the complexity of 3D vortex wake flows produced by nekton with hydrodynamically distinct propulsors.

KEY WORDS: Cephalopod, Jet propulsion, Fin motion, Volumetric velocimetry, Wake dynamics

INTRODUCTION

Squids swim using a dual-mode system involving a pulsed jet and complex fin motions, both of which are supported and powered by muscular hydrostats (Kier, 1989; Kier and Smith, 1985b; Kier and Thompson, 2003). The pulsed jet is produced by (1) expanding the mantle through a combination of radial muscle contraction, elastic recoil and flow-induced pressure differentials (Gosline and Shadwick, 1983; Gosline et al., 1983; Vogel, 1987), which brings water into the mantle through channels around the head, and (2) contracting the mantle via circular muscles, which drive a jet of water out of a funnel that is capable of vectoring the flow in any direction within a hemisphere below the body. The muscular hydrostatic fins are composed of three orientations of muscle fibers arranged above and below a median connective tissue fascia (Kier, 1989; Kier and Thompson, 2003) and produce complex flapping and traveling wave motions for stability control and thrust/lift generation, complementing the jet mechanism (Anderson and DeMont, 2005; Bartol et al., 2001b; Hoar et al., 1994; O'Dor, 1988; Stewart et al., 2010). Using this dual-mode system, squids are capable of remarkable locomotor flexibility. They can hover in place, change direction rapidly, brake, navigate structurally complex habitats, ascend or descend almost vertically, and swim forward (arms-first swimming) and backward (tail-first swimming) with apparent ease (Bartol et al., 2001a,b; Hanlon et al., 1983; Vecchione and Roper, 1991). Coordination of fin movements and the jet are essential for achieving the behaviors described above.

The ability to swim arms-first (forward swimming) and tail-first (backward swimming) is ecologically important for many squids (Fig. 1). Arms-first swimming is often employed to capture prey, investigate habitats and exhibit antagonistic displays (Bartol et al., 2001a,b; Foyle and O'Dor, 1988; Kier and Leeuwen, 1997; Messenger, 1968), whereas tail-first swimming is the preferred mode for cruising and high-speed escape jetting (Anderson and DeMont, 2000; Bartol et al., 2001a,b; O'Dor, 1988). During arms-first swimming, mantle refilling may be aided by the easier entry of water into the intake channels, since no directional change in water flow is necessary, as is the case for tail-first swimming. However, extensive funnel bending is also required to direct the jet rearward in the arms-first mode, presumably placing greater demands on the radial, longitudinal and circular muscles comprising the funnel than during tail-first swimming (Kier and Thompson, 2003). These demands may limit funnel bending at higher speeds and funnel aperture control, which may impact propulsive efficiency. The fins are also positioned differently in each mode, with the fins located at the leading edge during tail-first swimming and trailing edge during arms-first swimming. The advantages of these positions for propulsion and stability in squids are not fully known, but having control surfaces and propulsive mechanisms at leading and trailing edge locations, respectively, has been shown to be beneficial in other nektonic animals (Weihs, 2002).

The hydrodynamics of the squid jet have been well studied (Anderson and DeMont, 2000; Anderson and Grosenbaugh, 2005; Bartol et al., 2001b, 2008, 2009a,b; Johnson et al., 1972; O'Dor, 1988) but less is known about the hydrodynamics of the fins (Bartol et al., 2001b, 2008; Stewart et al., 2010). In many of these studies, digital particle image velocimetry (DPIV) was used to provide quantitative data on jet and fin flows (Anderson and Grosenbaugh, 2005; Bartol et al., 2008, 2009a,b; Stewart et al., 2010). One limitation of DPIV, however, is that it can only quantify flows in one plane at a time. Consequently, if fluid movements are outside the plane, as is the case with the jet and fins of squid, it is impossible to study wake patterns of these systems simultaneously. To address this limitation, many researchers study flows around the various propulsors at different times and infer 'average' flow patterns from temporally

[1]Department of Biological Sciences, Old Dominion University, Norfolk, VA 23529, USA. [2]Department of Mechanical Engineering, Southern Methodist University, Dallas, TX 75275, USA. [3]Department of Biology, Franklin and Marshall College, Lancaster, PA 17604, USA.

*Author for correspondence (ibartol@odu.edu)

Received 3 August 2015; Accepted 15 November 2015

Journal of Experimental Biology

Journal of Experimental Biology (2016) 219, 392-403 doi:10.1242/jeb.129254

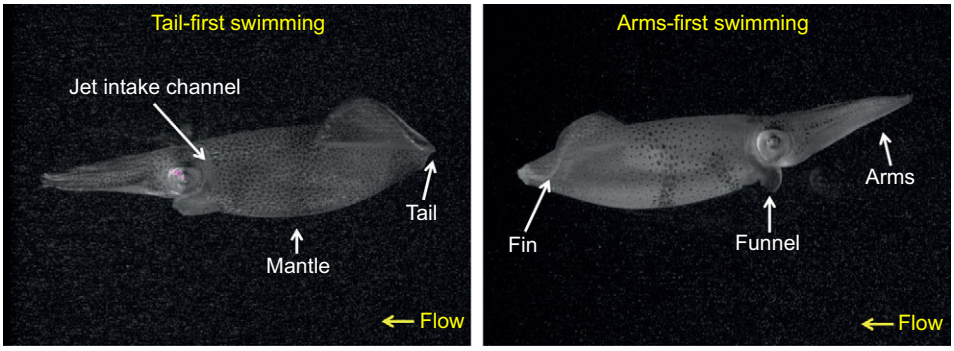

Fig. 1. Images of brief squid *Lolliguncula brevis* swimming tail-first (left) and arms-first (right). Squid swim using a combination of fin motions and pulsed jets directed using a highly maneuverable funnel.

distinct data. Although useful for determining overall force production, the lack of simultaneous information in this approach makes the study of jet/fin mode coordination impossible. For conventional DPIV, axisymmetry of the 3D vortex structures is typically assumed during impulse and energy calculations because it is not possible to quantify the 3D structure of the vortices in real time with this technique. As vortices in the wakes of animal systems are rarely axisymmetric and often convect into and out of the laser plane, true 3D flow visualization and quantification of vortex structures are needed for reliable force and efficiency calculations. Modifications to conventional DPIV, incorporating multiple simultaneous light sheets (Standen and Lauder, 2007), stereo-DPIV (Nauen and Lauder, 2002) and multi-plane scanning DPIV (Burgmann et al., 2006), do provide greater spatial resolution in planar cross-sections, but either the number of planes is too small or they are not sufficiently synchronized in time to provide a truly global picture of the flow.

For this study, we used a volumetric velocimetry technique, known as defocusing digital particle tracking velocimetry (DDPTV), which provides 3D, three-component velocity field measurements in a true volumetric domain (Couch and Krueger, 2011; Gharib et al., 2002; Kajitani and Dabiri, 2005; Pereira and Gharib, 2002, 2004; Pereira et al., 2006). This technique not only provides real-time volumetric quantitative data of flows around multiple propulsive systems but also provides a means of imaging 3D flow structures, such as looping and interconnected vortices. Vortex rings and their derivatives (vortex loops and chains) are central features of biological propulsion, as they are the critical coherent structures for momentum transfer. Vortex rings, in particular, are especially beneficial for propulsion because they entrain ambient fluid and accelerate the added mass of non-entrained fluid surrounding the vortex (Dabiri and Gharib, 2005b; Krueger and Gharib, 2003, 2005; Weihs, 1977). Thus, full volumetric quantification of these vortex ring structures as they are shed from multiple propulsors is critical for a comprehensive understanding of complex multi-mode systems like squids.

The goal of this study was to use DDPTV to study flows produced by the fins and jet of brief squid *Lolliguncula brevis* as they swim over a range of speeds. Because squid are capable of swimming in both arms-first and tail-first modes, we considered both swimming orientations in this study. Specifically, we sought to (1) visualize the suite of 3D flow structures produced by both the jet and fins, (2) calculate the force contributions of each propulsor and (3) calculate the propulsive efficiency for *L. brevis* at different speeds and directions. These data provide insight into how the jet and fins are used in coordination during steady swimming.

MATERIALS AND METHODS

Animals

Brief squid *Lolliguncula brevis* (Blainville 1823) [3.5–10.2 cm dorsal mantle length (DML), N=44] were captured by otter trawl near the Virginia Institute of Marine Science's Eastern Shore Lab (VIMS ESL) in Wachapreague, VA, USA. All captured animals were transferred to circular holding tanks (Angler Livewells, Aquatic Eco-Systems, Inc., Apopka, FL, USA) outfitted with battery-powered aerators, and transported to Old Dominion University's Marine Aquatics Facility. At this facility, animals were held in 400 gallon recirculating seawater systems with biological and mechanical filtration. Seawater was maintained at temperatures of 19–22°C and salinities of 30–35‰. A moderate current flow was provided in the holding tanks to promote active swimming, and squid were fed a diet of live *Palaemonetes pugio* and *Fundulus heteroclitos*. All animals were kept in the holding tanks for at least 72 h prior to experimentation.

Experiments

Each squid was placed in a water tunnel with a 15×15×44 cm working section [Model 502(s), Engineering Laboratory Design, Lake City, MN, USA] filled with seawater, matching conditions of the holding tanks and containing 50 µm light-reflective polyamide seeding particles (Dantec Dynamics, Skovlunde, Denmark). A V3V-8000 probe (TSI, Inc., Shoreview, MN, USA; three 12-bit, 2048×2048 pixel cameras) was positioned to the side of the tunnel. A 14×14×10 cm region of the test section was illuminated with two pulsed Nd:YAG lasers (LABest, Optronics, China), and paired DDPTV images (Δt=0.5–2.0 ms) of the flow around the squid were captured at 7 Hz. Identification of 3D particle locations and calculation of particle displacements were performed using INSIGHT 4G V3V software (TSI, Inc.), following protocols described in Pereira et al. (2000) and Troolin and Longmire (2010). On average, 100,000 particles were identified in each image with triplet yields (matches of particles among the three cameras in the probe) of ∼50,000–60,000 (∼50–60%). Using a relaxation method for particle tracking, which provides accurate results at low and high particle displacements and is more robust and efficient than nearest neighbor and neural network tracking methods (Pereira et al., 2006), approximately 18,000–25,000 particle vectors were obtained in the imaging volume. To obtain data about vorticity and vortex location, the vectors were interpolated onto a structured grid using a Gaussian weighting interpolation available in INSIGHT 4G V3V software. A voxel size of 8 mm, percentage overlap of 95% and smoothing factor of 1.5 were used in these experiments. A more detailed description of the DDPTV or V3V procedure may be found in Couch and Krueger (2011), Troolin and Longmire (2010) and Flammang et al. (2011a,b), with sensitivity analyses performed by Graff and Gharib (2008).

During DDPTV image capture, images from three Falcon high-speed cameras (Teledyne Dalsa, Inc., Waterloo, ON, Canada; 1400×1200 pixels, 100 frames s^{-1}) were collected, permitting

simultaneous collection of both 3D kinematic data from three views and 3D hydrodynamic data. The high-speed cameras were illuminated with halogen lights equipped with optical filters with low transmission at 532 nm. To prevent overexposure of frames from the pulsed Nd:YAG laser (wavelength 532 nm), each Falcon camera was outfitted with a notch filter to block 532 nm wavelengths. Similarly, the V3V-8000 probe was outfitted with optical filters that transmitted wavelengths of 532±5 nm so that only laser light illuminated the DDPTV CCD sensors. Two PCI NI-6602 timing boards, two BNC-2121 breakout boxes, and NI timing software (National Instruments, Austin, TX, USA) were used to send timing signals to the high-speed cameras, TSI synchronizer and BNC-565 pulse generator (Berkeley Nucleonics, San Rafael, CA, USA). The synchronizer and pulse generator in turn sent triggering signals to the V3V probe and Nd:YAG lasers, respectively.

Analysis

The high-speed video footage was used to measure accurate jet (refill and contraction) and fin (upstroke and downstroke) cycles, to determine squid positioning in the tunnel relative to the tunnel walls, and to calculate swimming velocities. Swimming velocities (U) were determined by measuring net displacement along the x-axis over complete jet or fin cycles and adding this to the background water tunnel speed. Because the squid body illuminated brightly under laser light, custom-designed masks were made in INSIGHT 4G V3V software to remove the squid body from each image prior to DDPTV processing. Velocity and vorticity fields were calculated using INSIGHT 4G V3V software and images were generated in Tecplot 360 (Tecplot, Bellevue, WA, USA). Matlab routines developed in-house were used to compute impulse ($\mathbf{I}$) associated with the vortical flows generated by the squid. Specifically, $\mathbf{I}$ of an isolated vortex was computed from:

$$\mathbf{I}/\rho = \frac{1}{2}\int_V \mathbf{x}\times\boldsymbol{\omega}\,\mathrm{d}V, \tag{1}$$

where $\mathbf{x}$ is the position vector, $\boldsymbol{\omega}$ is the vorticity vector ($\boldsymbol{\omega}=\nabla\times\mathbf{u}$, where $\mathbf{u}$ is the velocity vector), ρ is the fluid density, and the integral is computed over the volume of the vortex (Saffman, 1992). In the present study, the 3D volume surrounding the vortex of interest was selected using a graphical user interface (GUI) developed in-house in Matlab and the integral was computed over this volume to minimize the influence of measurement noise near the flow of interest. As impulse is the time integral of the force vector that generated the flow, the average thrust/lift vector (magnitude and 3D direction) was determined by dividing $\mathbf{I}$ by the period of the flow generation (T). Time-averaged jet thrust ($\overline{F}_{\mathrm{jt}}$) and fin thrust ($\overline{F}_{\mathrm{ft}}$) were calculated using:

$$\begin{aligned}\overline{F}_{\mathrm{jt}} &= -\mathbf{I}\cdot\hat{\mathbf{x}}/T,\\ \overline{F}_{\mathrm{ft}} &= -\mathbf{I}\cdot\hat{\mathbf{x}}/T,\end{aligned} \tag{2}$$

where $\hat{\mathbf{x}}$ is the unit vector opposite the direction of tunnel flow and T is either the fin cycle or the jet cycle period. The negative sign is included because Eqn 1 computes the fluid impulse and the impulse applied to the squid is in the opposite direction by Newton's Third Law. Additionally, because $\mathbf{I}$ is directed along the flow momentum, the angle of the jet was determined as $\arctan(I_y/I_x)$ where I_x and I_y are components of the impulse vector in the x and y coordinate directions, respectively. Similar to thrust, time-averaged lift forces from the jet ($\overline{F}_{\mathrm{jl}}$) and fin ($\overline{F}_{\mathrm{fl}}$) are computed as:

$$\begin{aligned}\overline{F}_{\mathrm{jl}} &= -\mathbf{I}\cdot\hat{\mathbf{y}}/T,\\ \overline{F}_{\mathrm{fl}} &= -\mathbf{I}\cdot\hat{\mathbf{y}}/T,\end{aligned} \tag{3}$$

where $\hat{\mathbf{y}}$ is the unit vector in the vertical direction.

Several approaches were used to calculate kinetic energy (E) of the wake. One approach using vorticity computes total kinetic energy from the 3D velocity field in a specified volume as:

$$E/\rho = \int \mathbf{u}\cdot(\mathbf{x}\times\boldsymbol{\omega})\,\mathrm{d}V - \int[(\mathbf{u}\cdot\mathbf{x})(\hat{\mathbf{n}}\cdot\mathbf{u}) - \frac{1}{2}u^2(\hat{\mathbf{n}}\cdot\mathbf{x})]\,\mathrm{d}S, \tag{4}$$

where $\hat{\mathbf{n}}$ is the outward unit vector on the surface of the specified region (Saffman, 1992), $u^2=|\mathbf{u}|^2$ is the square of the velocity magnitude, and the integration is taken over the same volume selected for computing the impulse $\mathbf{I}$. For an isolated vortex, as the surface becomes larger, the surface integral term in Eqn 4 vanishes and the result reduces to:

$$E/\rho = \int \mathbf{u}\cdot(\mathbf{x}\times\boldsymbol{\omega})\,\mathrm{d}V. \tag{5}$$

Eqn 5 allows the kinetic energy associated with specific vortices to be isolated, but the integrand is not guaranteed to be positive, so it can lead to inaccurate results if the data are noisy or if nearby vortices are too close so that the surface integral in Eqn 4 is not negligible. To avoid these potential shortcomings, kinetic energy in the present study was computed using Eqn 4, which is mathematically equivalent to:

$$E/\rho = \frac{1}{2}\int |\mathbf{u}|^2\mathrm{d}V, \tag{6}$$

where $|\mathbf{u}|$ is the velocity magnitude. The advantage of this approach is that it will always give a positive value for E. The disadvantage is that it does not necessarily isolate the E associated with only the vortex of interest because of the influence of the surface integral term. One consequence is that Eqn 4 provides a conservative measurement of the kinetic energy because the selected region can contain flow from neighboring vortices and any background noise in the selected region will increase the computed energy value. In application of Eqn 4, the background flow velocity was subtracted from the local velocity vector prior to computing the kinetic energy because only the excess kinetic energy is relevant for propulsive efficiency.

The rate of excess kinetic energy shed by the jet and fins ($\dot{E}_{\mathrm{j}}$ and $\dot{E}_{\mathrm{f}}$, respectively) was computed by dividing E by the appropriate jet or fin cycle period. Propulsive efficiency (η) was determined using the following equation:

$$\eta = \frac{\overline{F}_{\mathrm{jt}}U + \overline{F}_{\mathrm{ft}}U}{\overline{F}_{\mathrm{jt}}U + \overline{F}_{\mathrm{ft}}U + \dot{E}_{\mathrm{j}} + \dot{E}_{\mathrm{f}}}. \tag{7}$$

RESULTS

Wake patterns

Vortex rings were prominent wake features for brief squid *L. brevis*. At low speeds (<1.5 DML s^{-1}), short flow pulses with vortex rings were frequently produced by the fins and jet during both arms-first and tail-first swimming (Fig. 2). At intermediate speeds (1.5–3.0 DML s^{-1}), vortex rings were also common, but vorticity patterns were more complex and often involved interconnected ring structures. In general, the highest diversity of vortex-wake flows was observed in this intermediate speed range. For arms-first swimming, vortex rings shed from the fins were frequently observed

Journal of Experimental Biology (2016) 219, 392-403 doi:10.1242/jeb.129254

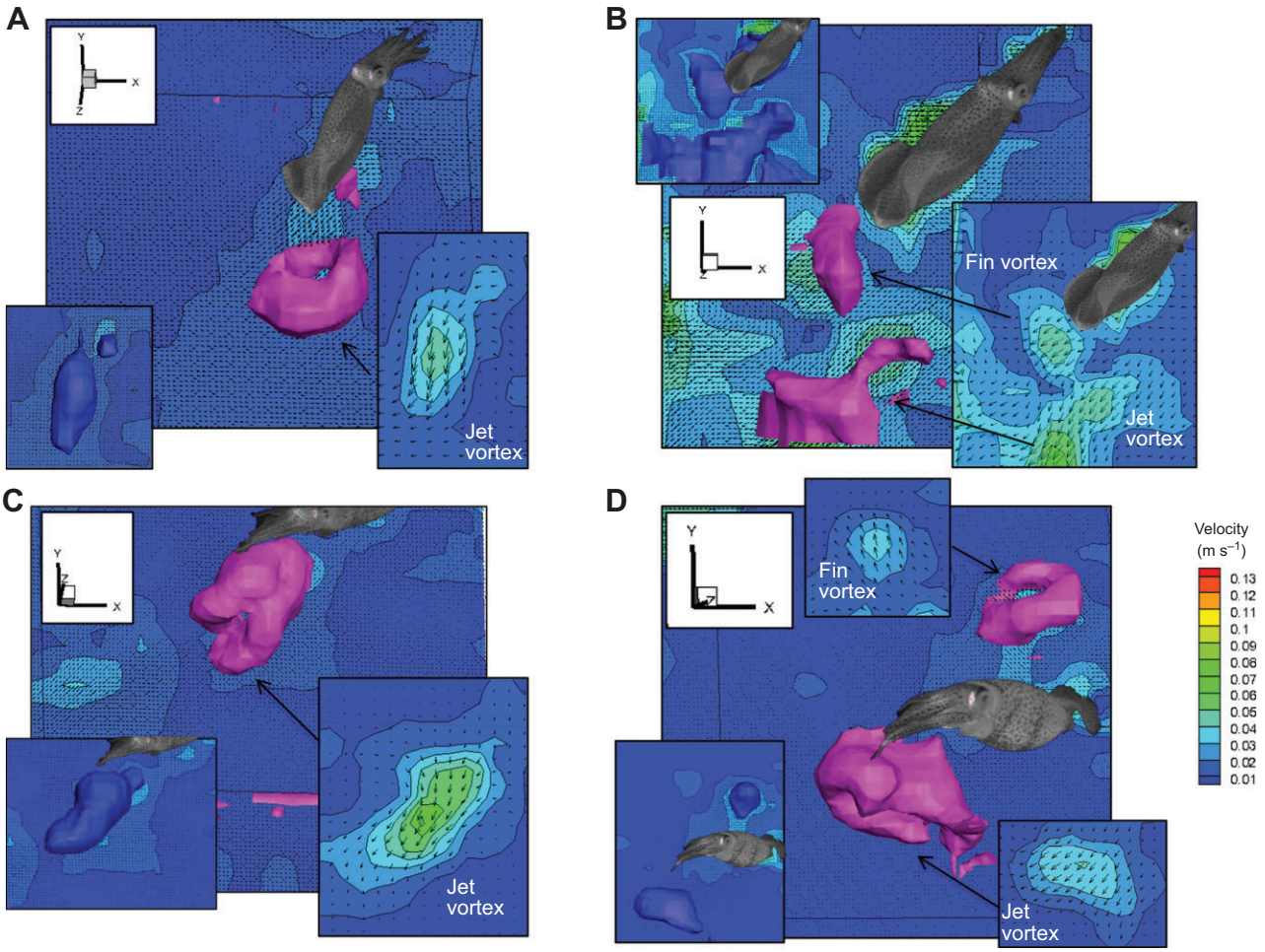

Fig. 2. *Lolliguncula brevis* swimming in both orientations. Defocusing digital particle tracking velocimetry (DDPTV) images of brief squid swimming at low speeds [<1.5 dorsal mantle lengths (DML) s^{-1}] in the arms-first (A,B) and tail-first (C,D) orientations. At these speeds, short pulses with vortex rings were common from both the fins and jet. Vorticity magnitude isosurfaces are pink, velocity magnitude isosurfaces are blue, and insets with arrows are velocity slices; background flow (tunnel speed) was subtracted from the images, with flow moving from right to left.

and sometimes merged with, or were in close proximity to, jet vortex rings (Fig. 3). During tail-first swimming, isolated, interconnected and closely pulsed vortex rings were frequently produced by the jet, while the fins commonly produced more elongated regions of concentrated vorticity (Fig. 4), though isolated vortex rings were also observed (e.g. see Fig. 4C). In many cases, the fins produced significant lift and drag signatures. For example, downward and rightward tilted vectors in the fin vorticity insets of Fig. 4D,E illustrate lift and drag components, respectively. At high speeds (>3.0 DML s^{-1}), jet flows dominated with limited fin propulsive input (and activity in general). Arms-first swimming at high speeds frequently involved rapidly pulsed vortex rings (Fig. 5). High-speed tail-first swimming often involved elongated regions of jet vorticity with ring elements (Fig. 6). A leading edge vortex ring with a trailing jet of concentrated vorticity (Fig. 6A) was a commonly observed pattern. Evidence of ring elements within the jet vorticity was widespread (Fig. 6B). Rapidly pulsed isolated vortex rings were also observed (Fig. 6C,D), as in the arms-first case, but these were rarer than elongated regions of concentrated vorticity with leading rings, i.e. patterns illustrated in Fig. 6A,B.

Force production

The fins and jet both contributed to thrust to varying degrees, with the fins and jet contributing 0–83% and 17–100% of the total thrust, respectively, for steady swimming. For both swimming orientations, jet angle with respect to the *x*-axis (horizontal) decreased with increased speed (linear regression: arms-first: R^2=0.33, P=0.005; tail-first: R^2=0.18, P=0.003; Fig. 7A,D). Jet thrust became increasingly important as swimming speed increased, with fin thrust contributions being negligible at all speeds >4.5 DML s^{-1} (Figs 7, 8). In the majority of sequences, the jet contributed significantly more to thrust than the fins in both swimming orientations, and the proportion of jet thrust relative to total thrust increased as swimming speed increased (Fig. 9; linear regression: R^2=0.40, P=0.015). During both arms-first and tail-first swimming, jet thrust per unit body length increased with speed (linear regression: arms-first: R^2=0.58, P<0.0001; tail-first: R^2=0.66, P<0.0001), but no consistent relationship between jet lift per unit body length and swimming speed was observed for either orientation (Fig. 7).

During both arms-first and tail-first swimming, several sequences with negative fin thrust (drag) production were observed, with negative fin thrust being more common during tail-first than during arms-first swimming (Fig. 8A,C). When only positive thrust was considered for the range of speeds when the fins were active (0–4.5 DML s^{-1}), there was no clear reduction in fin thrust as swimming speed increased for arms-first swimming, but there was a reduction in fin thrust with increasing swimming speed for tail-first swimming (linear regression: tail-first: R^2=0.37, P=0.013;

Journal of Experimental Biology (2016) 219, 392-403 doi:10.1242/jeb.129254

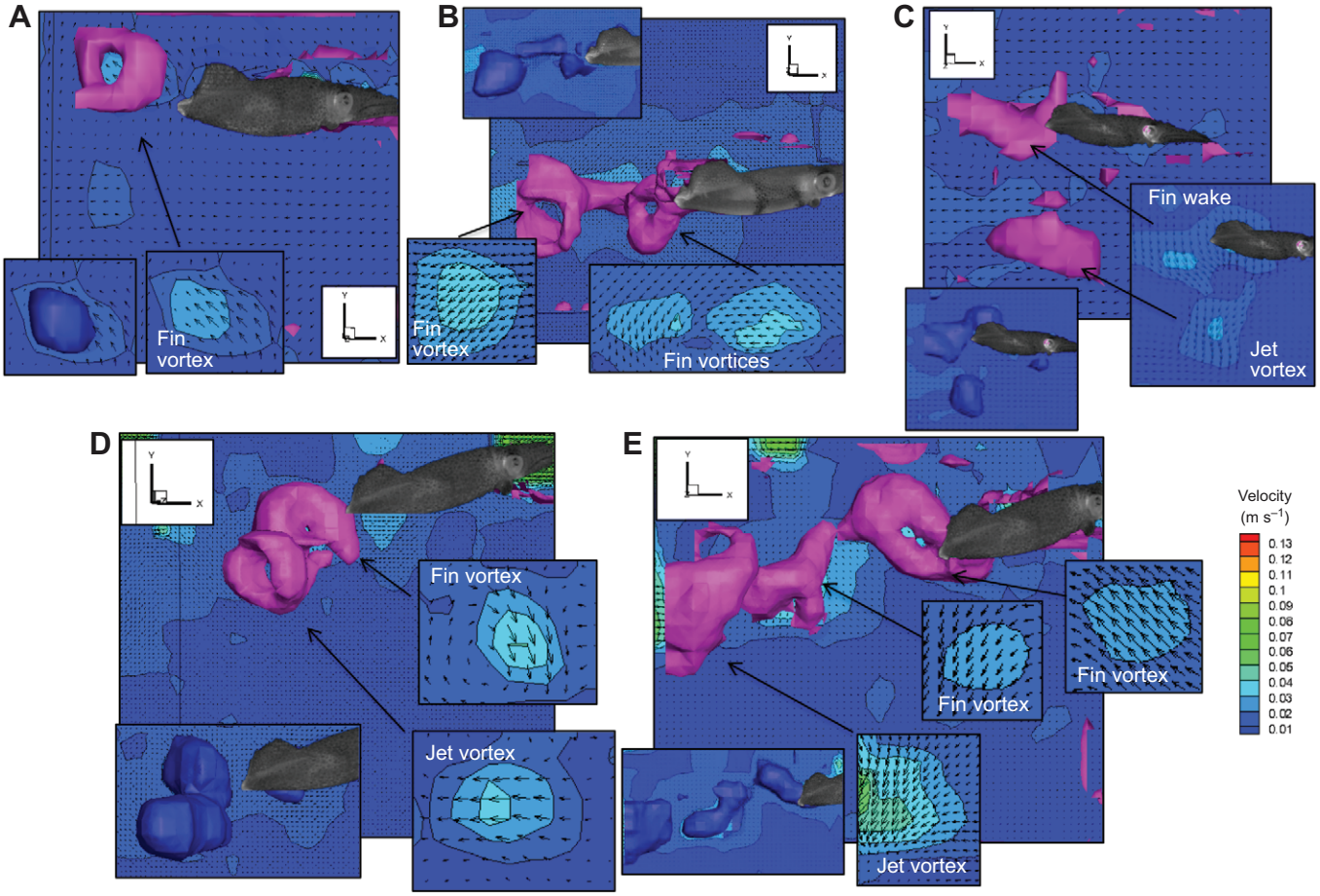

Fig. 3. DDPTV images of *L. brevis* swimming at intermediate speeds in the arms-first orientation. At intermediate speeds (1.5–3.0 DML s^{-1}, A–E), vortex rings were common but vorticity patterns were complex and there were often more interactive effects between fin and jet flows (e.g. D,E). For description, see Fig. 2.

Fig. 8). Negative lift production was also observed for some sequences in both arms-first and tail-first swimming. When only positive lift was considered for the range of speeds when the fins were active, there was a significant decrease in lift production as swimming speed increased for arms-first swimming (linear regression: arms-first: R^2=0.33, P=0.015), but a significant relationship was not detected for tail-first swimming (linear regression: tail-first: R^2=0.20, P=0.052). However, for both orientations, lift production was higher for speeds <2.0 DML s^{-1} than for higher speeds.

Propulsive efficiency

When fin activity was factored into propulsive efficiency calculations (as opposed to only considering the pulsed jet), overall propulsive efficiency generally increased 2–19% in cases when the fins and jet were both active. However, in some cases, propulsive efficiency decreased. The decrease was generally low (<3%), but in some sequences the decrease in propulsive efficiency approached 11%. Mean propulsive efficiency was 62.2±20.9% (mean±s.d.) for arms-first swimming and 66.5±19.1% for tail-first swimming. No significant difference in these efficiencies was detected (2-tailed t-test, d.f.=107, P=0.388; Fig. 10C). Propulsive efficiency increased as swimming speed increased for both orientations (logarithmic regression: arms-first: R^2=0.33, P<0.001; tail-first: R^2=0.30, P<0.001; Fig. 10). Propulsive efficiency for swimming sequences with jet wakes having clearly observable isolated vortex rings (mean η=78.6±7.6%) was significantly greater than that for swimming sequences with jet wakes having clearly observable elongated regions of concentrated vorticity (mean η=67.9±19.2%; 2-tailed t-test, d.f.=34, P=0.044). Moreover, propulsive efficiencies for fin-dominated sequences (mean η=57.7±17.9%) were significantly lower than those for jet-dominated sequences (mean η=68.1±19.6%; 2-tailed t-test, d.f.=107, P=0.016).

DISCUSSION

Studying locomotion in squids is particularly challenging because they swim both arms-first and tail-first and employ a dual-mode propulsive system involving a vectored jet and muscular hydrostatic fins. Here, we provide the first 3D hydrodynamic dataset of squid swimming in both directions, with full 3D visualizations of wake features, 3D force measurements and 3D propulsive efficiency measurements.

Fin and jet wake patterns

Two principal hydrodynamic jet modes have been identified in juvenile and adult *L. brevis* in previous studies: (1) jet mode I, where the ejected fluid rolls up into an isolated vortex ring for each jet pulse, and (2) jet mode II, where the ejected fluid develops into a leading vortex ring that separates or pinches off from a long trailing jet for each pulse (Bartol et al., 2008, 2009b). These two modes, which were identified in two-dimensional slices using

Journal of Experimental Biology (2016) 219, 392-403 doi:10.1242/jeb.129254

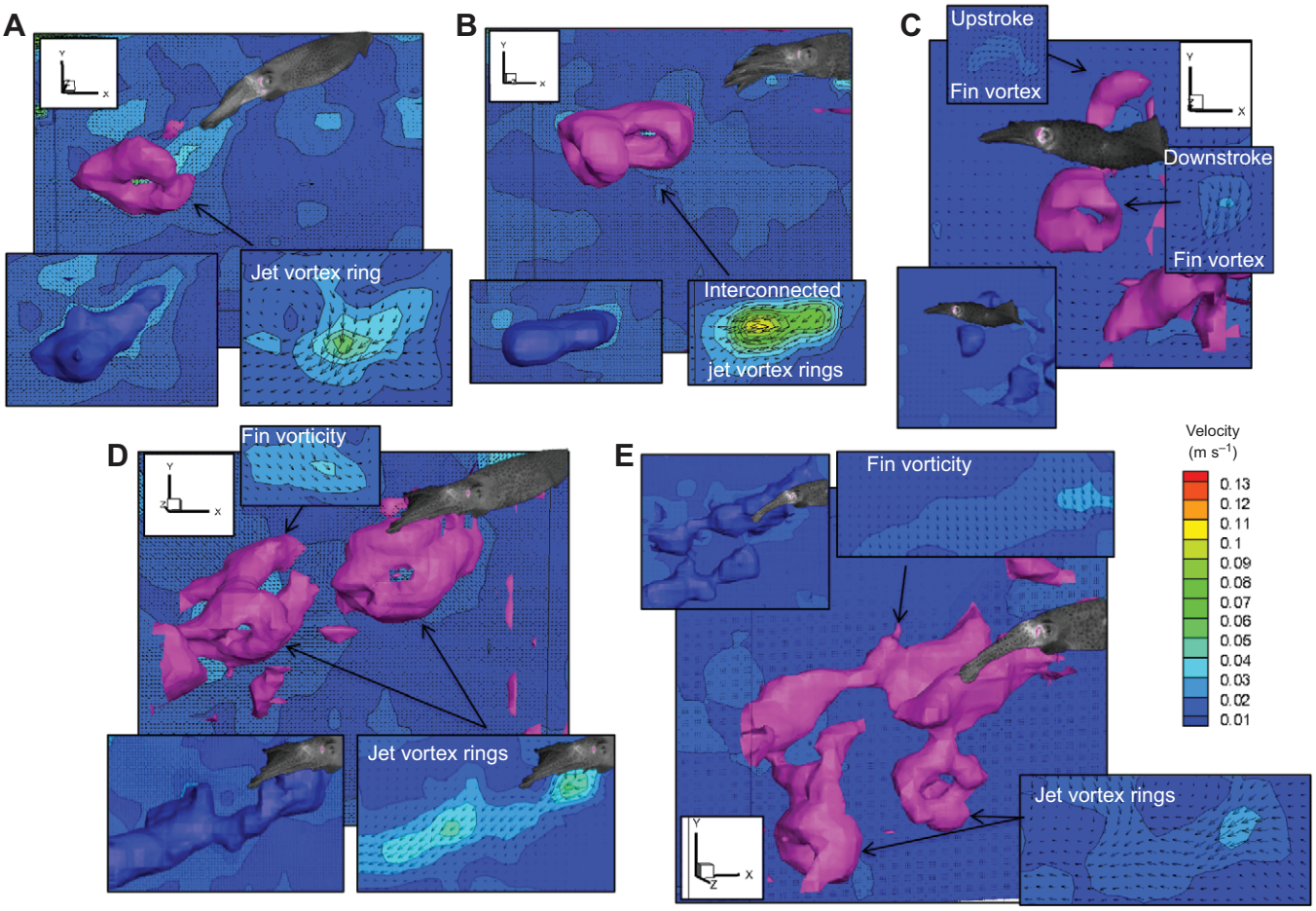

Fig. 4. DDPTV images of *L. brevis* swimming at intermediate speeds in the tail-first orientation. At intermediate speeds (1.5–3.0 DML s^{-1}, A–E), vortex rings were also common but vorticity patterns were more complex and there were often more interactive effects between fin and jet flows (e.g. D,E). For description, see Fig. 2.

DPIV, were also detected in their 3D forms in the current study (e.g. Fig. 4A, Fig. 6A). We observed that the shorter pulsed jet rings were generally more common at low speeds and longer jets were more apparent at high speeds. Nevertheless, as in previous studies (Bartol et al., 2008, 2009b), both patterns were observed to some degree at all speeds, with isolated vortex rings seen at speeds as high as 8.0 DML s^{-1} (33.6 cm s^{-1}) and elongated jets seen at speeds as low as 1.3 DML s^{-1} (5.2 cm s^{-1}). In addition to jet modes I and II, other patterns were observed that have not been reported previously, including interconnected vortex ring jets (e.g.

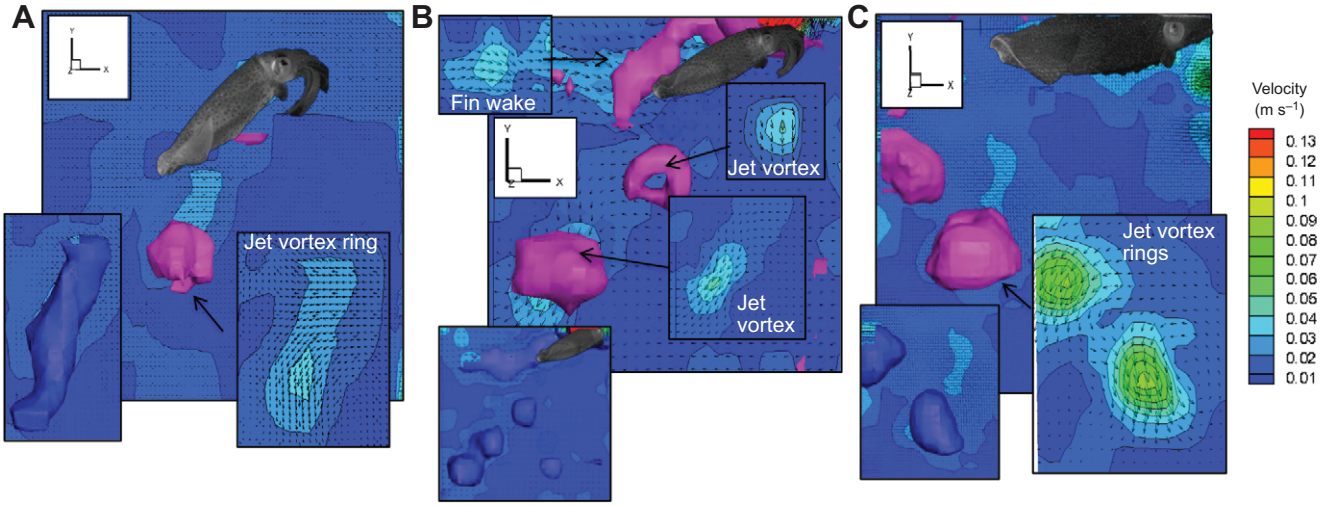

Fig. 5. DDPTV images of squid swimming at high speeds in the arms-first orientation. At high speeds (>3.0 DML s^{-1}, A–C), jet flows dominated with little fin input and most sequences involved rapidly pulsed vortex rings. For description, see Fig. 2.

Journal of Experimental Biology (2016) 219, 392-403 doi:10.1242/jeb.129254

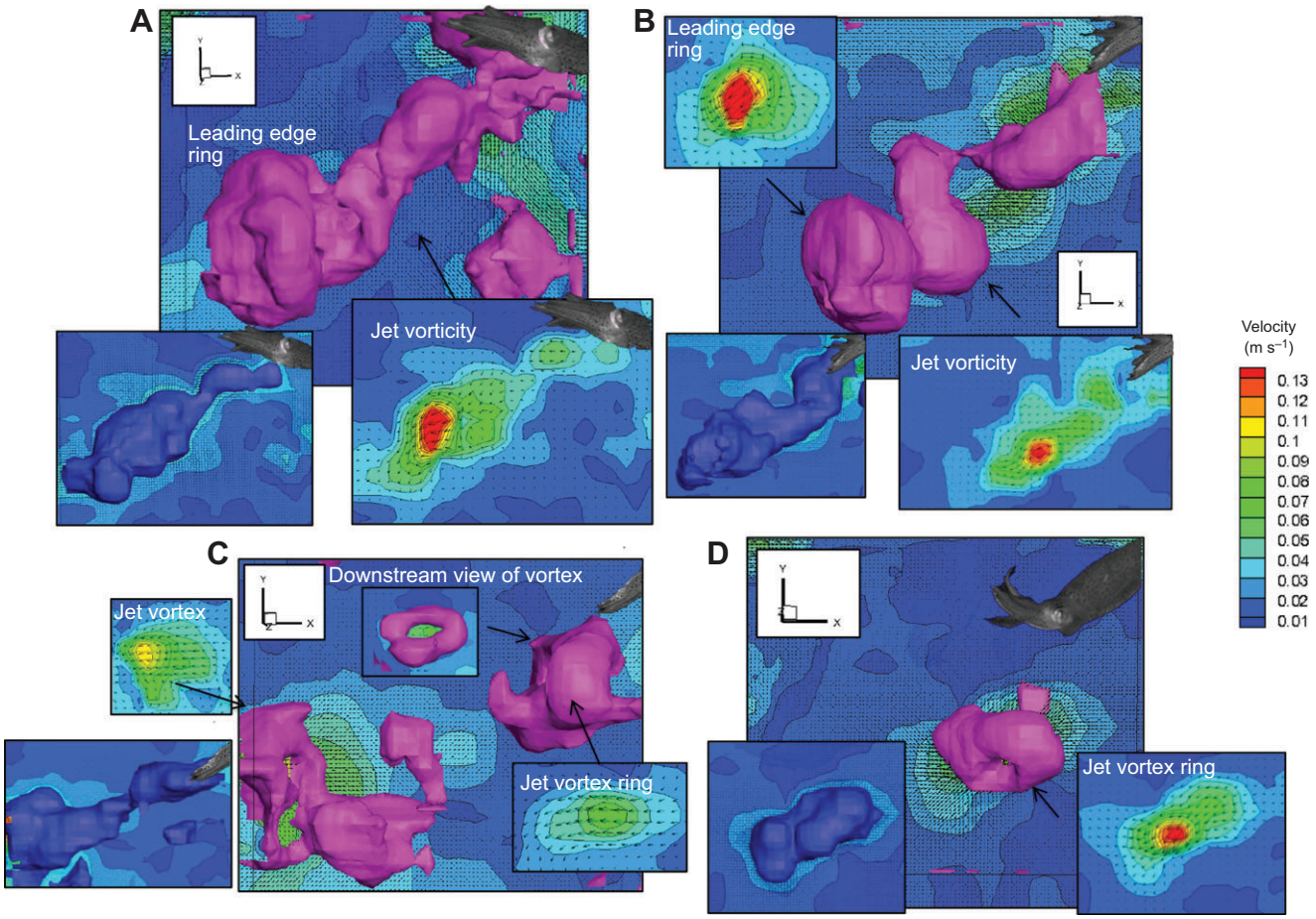

Fig. 6. DDPTV images of squid swimming at high speeds in the tail-first orientation. At high speeds (>3.0 DML s^{-1}, A–D), jet flows dominated with little fin input and most sequences involved elongated regions of concentrated vorticity with ring elements, especially at the leading edge (A,B). Rapidly pulsed vortex rings (C,D) were also observed, though they were less common. For description, see Fig. 2.

Fig. 4B) and long jets with ring elements (e.g. Fig. 4D, Fig. 6B). These patterns are particularly interesting because they suggest that jet expulsion is more complex than previously thought, with pulsatile components occurring during the jet expulsion phase. These pulsations may be due to mantle contraction force variation and/or funnel aperture control, as observed in squids in other studies (Anderson and DeMont, 2000; Bartol et al., 2001b, 2009b; O'Dor, 1988).

While turbulent 3D jets with no apparent vortex ring structures were sometimes observed, jets with 3D vortex ring structures, whether in the form of isolated rings or elements of longer jets, were the most common for *L. brevis* (3.5–10.2 cm DML). This is consistent with wake visualizations for juvenile/adult *L. brevis* (Bartol et al., 2001b, 2008, 2009b) and paralarval *Doryteuthis* (formerly *Loligo*) *pealeii* (Bartol et al., 2009a). Jets with vortex ring structures are not consistently found in all squid, however. In larger, long-finned squid *D. pealeii* (~27 cm DML), jets are highly turbulent with rare/sporadic vortex ring formation (Anderson and Grosenbaugh, 2005). These differences suggest that there may be some intraspecific or size differences in jet wake patterns among squids and possibly a transition in jet structure at body Reynolds numbers (Re_{body}) of ~22,000 given that Re_{body} of all *L. brevis* were <16,000 and Re_{body} for all adult *D. pealeii* were >22,000.

As many as four fin wake modes have been detected in *L. brevis* (using 2D flow field measurements): two are used during arms-first swimming and all four are used during tail-first swimming (Stewart et al., 2010). These fin flow patterns involve either (1) isolated vortex rings produced during downstrokes, upstrokes, or both, or (2) interconnected vortex structures. Both of these categories of flow patterns were observed in the present study, with isolated rings being illustrated in Fig. 2B,D, Fig. 3A,C, Fig. 4C, and interconnected ring structures being represented in Fig. 3B,E. Stewart et al. (2010) noted that interconnected ring structures were the most common pattern produced by fins for arms-first swimming, which is consistent with our results. Unlike Stewart et al. (2010), however, we found that isolated rings and longer regions of concentrated vorticity rather than well-defined interconnected ring structures were most prevalent in fin wakes during tail-first swimming. Greater fin flow diversity was also detected during arms-first swimming than tail-first swimming, the orientation with the greatest number of fin modes reported by Stewart et al. (2010). These differences may be due to the difficulty in visualizing and quantifying some flows when squid swim in the tail-first orientation using the DDPTV approach. To eliminate false flows driven by laser illumination of the body and fins, body features were masked out prior to processing. While this masking technique had little impact on flows shed from the fins during arms-first swimming or even isolated vortex rings produced by the fins during tail-first swimming, which tended to move away from the body, it likely impacted visualization and quantification of interconnected vortex structures, as these often remained adjacent to the mantle. During mask removal, all particles falling between the squid body and camera along the *z*-axis (the camera viewing

Journal of Experimental Biology (2016) 219, 392-403 doi:10.1242/jeb.129254

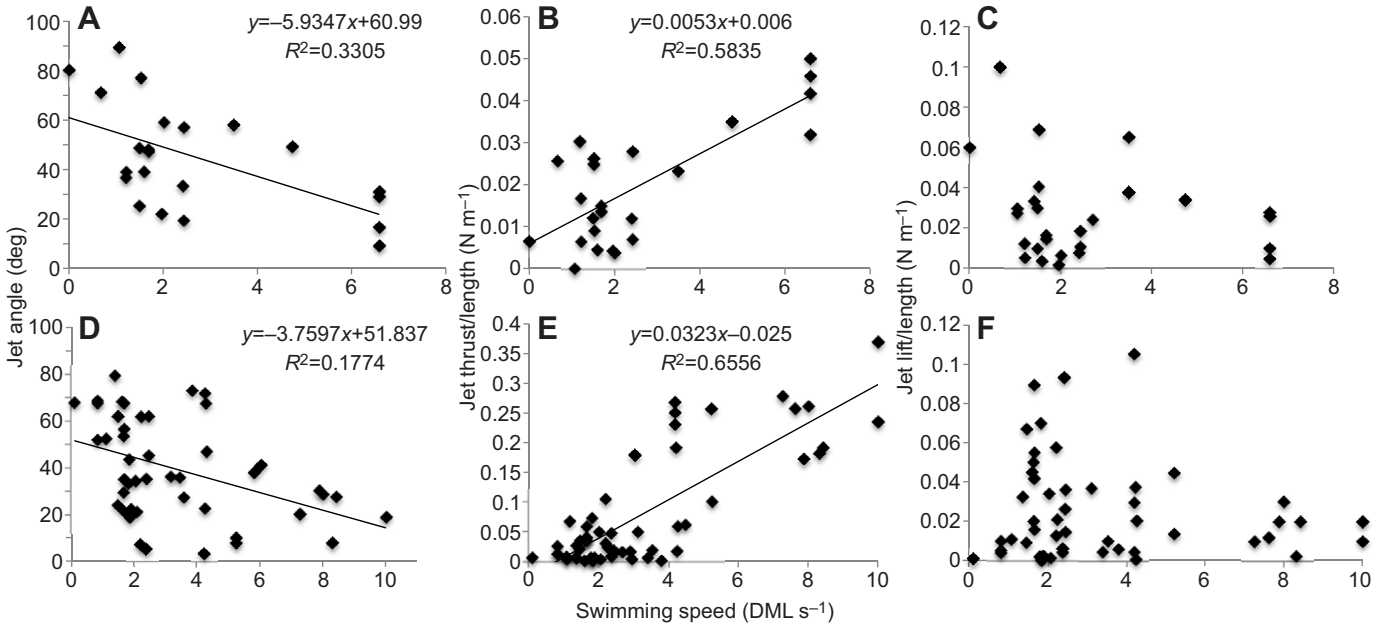

Fig. 7. Jet angle, thrust and lift as a function of speed for *L. brevis* swimming in both orientations. Jet angle (A,D), jet thrust (B,E) and jet lift (C,F) are plotted against swimming speed for arms-first (upper row) and tail-first (bottom row) swimming. Force was normalized to body length and swimming speed is expressed in DML s^{-1} to account for the different sizes of squid considered. No significant relationship between jet lift and swimming speed was detected.

direction) are removed from the processing field. A 3D masking technique to remove the squid body but not the illuminated particles in front of it is currently under development at TSI, Inc. (D. Troolin, personal communication). This software enhancement should improve the quality of future datasets and provide a more complete picture of flows very close to the body.

Drag wakes behind the fins (e.g. Fig. 4D,E, Fig. 5B) were common in the present study. This finding is consistent with previous studies that found that the fins produce drag during 38% of the swimming speeds in the arms-first mode and 17% of the swimming speeds in the tail-first mode (Stewart et al., 2010). Extending a fin or fins outward to produce negative thrust (drag) assists with dynamic stability and maneuverability, as demonstrated in other nekton (Fish, 2002; Webb, 2002; Weihs, 2002). Although recoil motions were not measured in the present study, drag-based fin flows were widespread during steady swimming in which the squid held position within the working section with minimal observable pitching, rolling and yawing. Having the fins positioned a considerable distance from the center of mass, as is the case for *L. brevis*, certainly facilitates torque corrections, even through small fin movements. Stability adjustments are especially effective when the fins are positioned at the leading edge (Weihs, 2002), which may be a reason for the greater occurrences of negative fin thrust during tail-first relative to arms-first swimming in the present study. Slight banking maneuvers whereby the squid moved from one side of the working section to the other were also associated with pronounced fin drag profiles, suggesting the fins play an integral role in turning. Indeed, fin braking is essential for high agility (rapid turning) and high maneuverability (tight turning) in cephalopods based on recent kinematic and hydrodynamic measurements (Jastrebsky et al., in press). The frequent presence of drag wakes behind the fins in the present study provides further evidence that the fins are integral elements for stabilization and steering, as demonstrated by Stewart et al. (2010) and suggested by others (Anderson and DeMont, 2005; Bartol et al., 2001a,b, 2008, 2009b; Hoar et al., 1994; O'Dor, 1988; O'Dor and Webber, 1991; Webber and O'Dor, 1986).

Fin and jet coordination

One important finding of this study was that flow contributions of the fins and jet change with speed in *L. brevis*. At low speeds (<1.5 DML s^{-1}), the fins and jet were active, with isolated vortex ring formation from both propulsors being common. The observed downward vectoring of the jet at lower speeds was expected, given that these animals are negatively buoyant and thus must generate forces to counteract their body weight (Bartol et al., 2001a,b), especially at low speeds when dynamic lift forces are low. The high spatial separation of fin and jet flows is also not unexpected given the high mantle angle of attack and downward directed jets at low speeds, behavioral patterns that have been observed in other studies of *L. brevis* (Bartol et al., 2001a,b, 2008, 2009b). These high mantle and jet angles contribute to greater spatial separation of fin and jet flows, whereas lower mantle and jet angles at intermediate and high speeds produce fin and jet flows that are closer together, with more opportunity for jet/fin flow interactions. Indeed, the high diversity in vortex-wake flows at intermediate speeds (1.5–3.0 DML s^{-1}) was a product of significant interactions between fin and jet flows. For arms-first swimming, vortex ring shedding from the fins was frequently observed, and at times, these flows merged with or were in close proximity to jet vortex rings. These interactions were more prevalent than at lower speeds because the funnel tended to direct the jet more horizontally toward the direction of fin wake shedding at intermediate speeds, when less downward-directed force is needed. During tail-first swimming, isolated, interconnected and closely pulsed vortex rings were frequently produced by the jet, while the fins produced more elongated regions of concentrated vorticity, often with significant lift and drag signatures to aid with counteracting negative buoyancy and stabilization. Again, significant interactions between fin and jet flows were present as the jet was directed closer to fin flow wakes than at lower speeds.

The observed heavy dependence on the jet at high speeds, i.e. speeds >3 DML s^{-1}, is consistent with previous studies (O'Dor, 1988; Bartol et al., 2001b). The absence of significant fin thrust at high speeds (i.e. >4.5 DML s^{-1}) may result from limitations of the

Journal of Experimental Biology (2016) 219, 392-403 doi:10.1242/jeb.129254

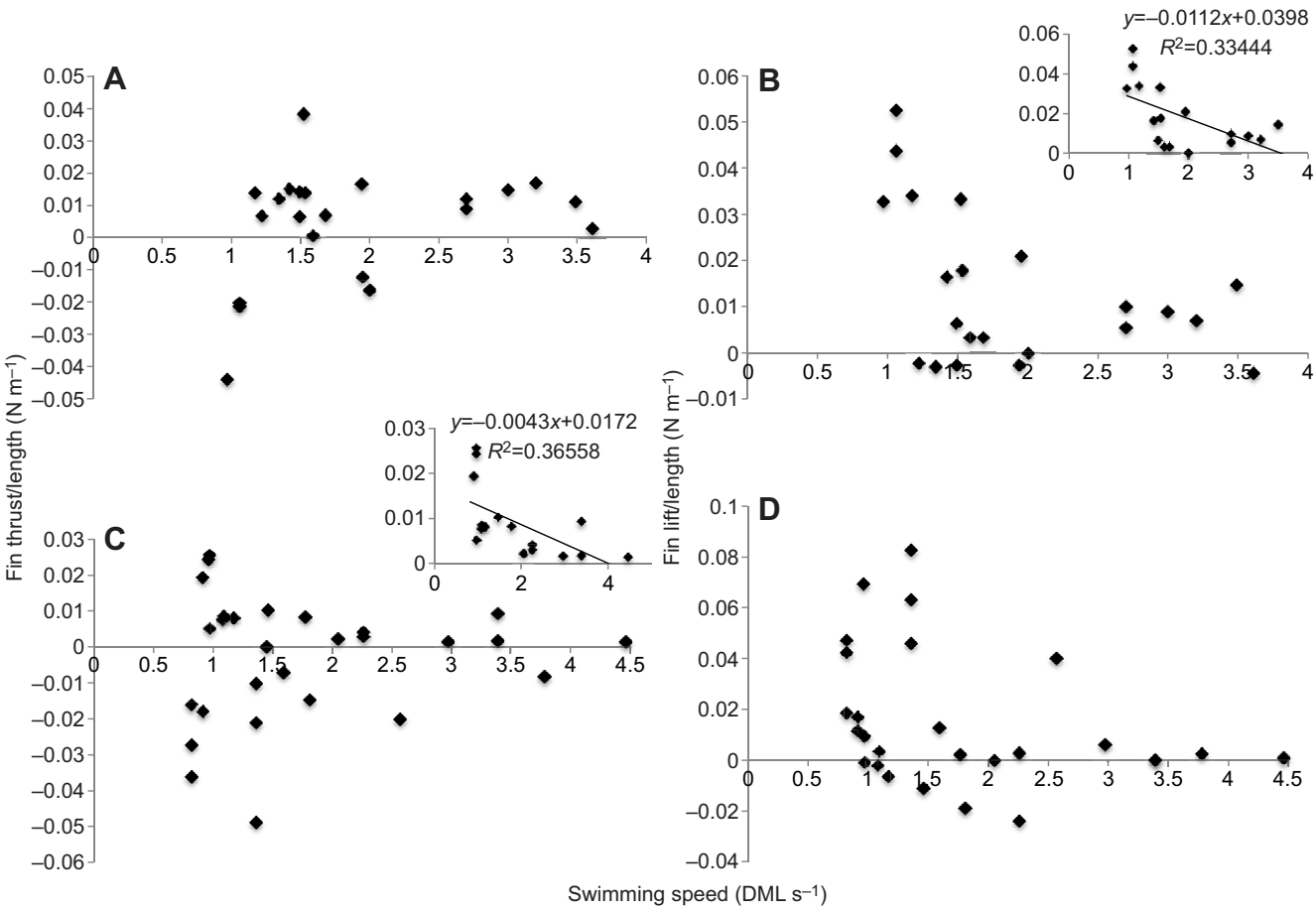

Fig. 8. Fin thrust and lift as a function of speed for *L. brevis* swimming in both orientations. Fin thrust (A,C) and fin lift (B,D) are plotted against swimming speed for arms-first (upper row) and tail-first (bottom row) swimming. Force was normalized to body length and swimming speed is expressed in DML s^{-1} to account for the different sizes of squid considered. Insets denote significant regressions for positive force data.

fin musculature. The speed of movement and force output of the muscular hydrostatic fins of squid (Kier and Smith, 1985a, Kier, 1988, 1989) are determined by the contractile properties of the fin muscle fibers, though fin connective tissue fibers limit the range of motion and permit elastic potential energy storage and return (Kier, 1989; Johnsen and Kier, 1993). In contrast, the fins of fishes are composed of rigid lever systems, and fin speed and force output can be adjusted over evolution by altering the length of the input lever and/or muscle contractile properties. Squid fins lack a rigid lever system, and thus constraints on the ability of fin musculature to produce high force at the high shortening velocities required during rapid swimming (Kier, 1989; O'Dor and Webber, 1991) may underlie the observation that many squids wrap their fins around the mantle at very high swimming speeds (Bartol et al., 2001b; Hoar et al., 1994; O'Dor, 1988).

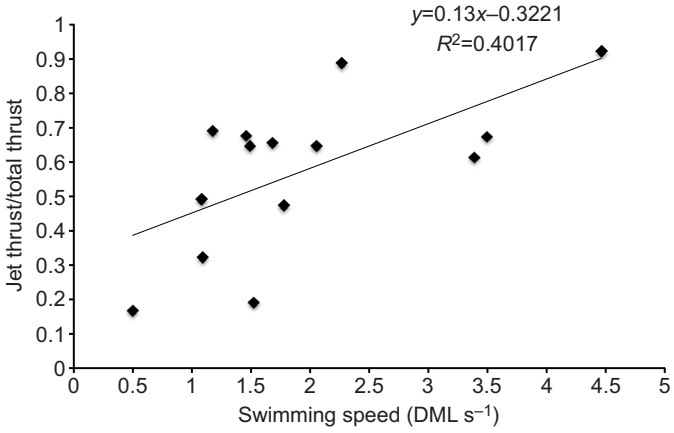

Fig. 9. Ratio of jet to total thrust as a function of swimming speed. Only those sequences where both clear fin and jet flows were quantifiable using DDPTV are considered here. Jet thrust becomes increasingly important with swimming speed, and at all speeds exceeding 4.5 DML s^{-1}, fin thrust contributions are negligible.

The high variability in fin and jet contributions to thrust is consistent with previous studies. By moving a laser sheet back and forth from the jet to the fins within short temporal windows, Bartol et al. (2008) were able to use DPIV to calculate fin and jet thrust contributions. Their results demonstrated that the jet and fins contribute ~17–96% and ~5–83% of the overall thrust, respectively, for *L. brevis* (4.6–6.2 cm DML) swimming at 1.1–1.7 DML s^{-1}. These measurements are very similar to 3D velocimetry measurements reported here, with the jet contributing 17–100% of total thrust, and the fins contributing 0–83% of the total thrust for *L. brevis* (3.5–10.2 cm DML) swimming over a broader range of speeds (0–10 DML s^{-1}). Using kinematic data and force balance calculations, Bartol et al. (2001b) reported fin thrust contributions of 0–55% and jet contributions of 45–100% for *L. brevis*. Collectively, these data suggest that there is great flexibility in how the fins and jet are employed, with both propulsors being capable of producing considerable thrust, at least at low/intermediate speeds.

Journal of Experimental Biology (2016) 219, 392-403 doi:10.1242/jeb.129254

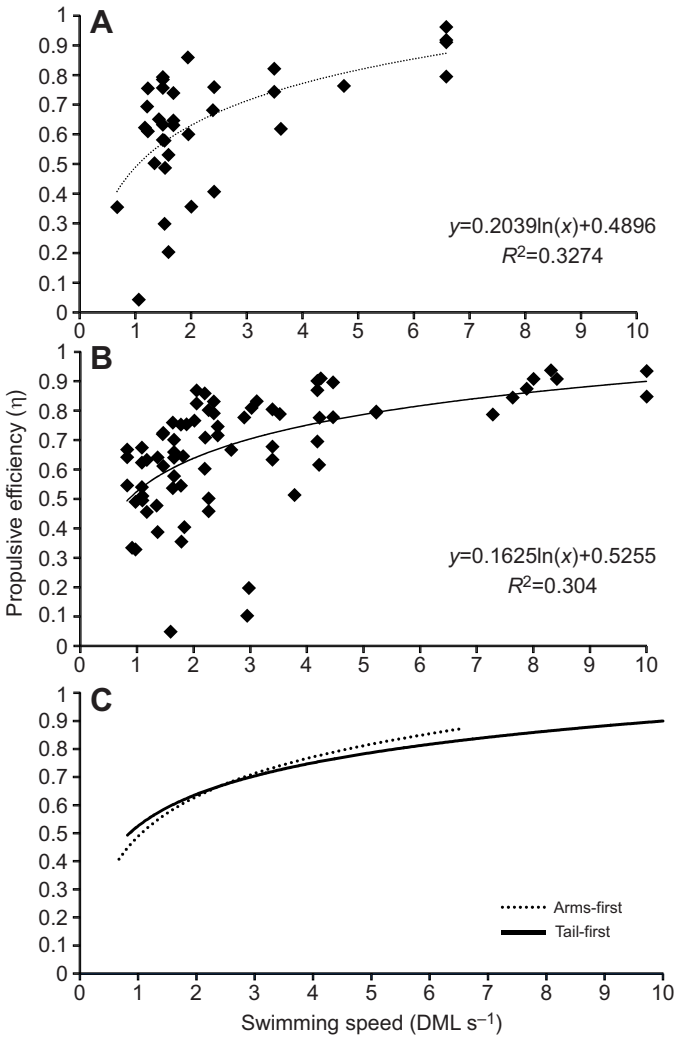

Fig. 10. Propulsive efficiency η as a function of swimming speed for *L. brevis* swimming in both orientations. (A) Arms-first swimming; (B) tail-first swimming; and (C) combined swimming.

Based on the results of the present study, the importance of the jet for thrust contributions increases as swimming speed increases, which is reasonable given the fin muscle limitations noted above. Over the speed range where the fins were employed for thrust (0–4.5 DML s^{-1}), no clear decrease in fin thrust was observed for arms-first swimming, while a clear decrease in fin thrust was observed for tail-first swimming. These results seemingly do not fully agree with Stewart et al. (2010), who found that although no clear increase in fin thrust with speed occurs during arms-first swimming, fin thrust does increase with speed between 0.2 and 1.9 DML s^{-1} during tail-first swimming. However, the present study considers a broader swimming speed range (0.8–4.5 DML s^{-1}) for tail-first swimming, with low thrust values that drive the relationship falling outside the range considered by Stewart et al. (2010). When similar speed ranges are considered, the differences are less apparent. Although the observed differences in speed/fin thrust relationships for arms-first and tail-first swimming in the present study could be, in part, a product of flow quantification limitations mentioned earlier for tail-first swimming, it is more likely a reflection of greater reliance on the fins for thrust during arms-first swimming. Indeed some previous studies have reported decreased fin frequency and amplitude with speed (for speeds where the fins were used) for tail-first swimming but not for arms-first swimming in *L. brevis* (Bartol et al., 2001b). This greater reliance on fins in the arms-first mode may be a product of funnel muscle constraints. During arms-first swimming, the funnel needs to bend extensively to direct jet flows rearward, which requires greater shortening by the radial muscles to prevent kinking and aperture constriction and ventral longitudinal muscles to maintain funnel curvature (Kier and Thompson, 2003). Limiting constriction and kinking is especially important because any decrease in funnel diameter (D) will lead to significant reductions in volume flux (and thrust); volume flux scales with D^4 for laminar pipe flow or $D^{5/2}$ for fully rough turbulent pipe flow (Munson et al., 2009). Reducing funnel bending and directing the jet less horizontally while relying more heavily on fins for thrust would certainly alleviate radial/longitudinal muscle requirements.

This study demonstrates that the fins are important for lift production at low speeds (<2.0 DML s^{-1}) but become less important at higher speeds. Other studies have also indicated the importance of fin lift production at low speeds (Anderson and DeMont, 2005; Bartol et al., 2001a,b; Hoar et al., 1994; Stewart et al., 2010). Lift production is especially important at low speeds when dynamic lift forces are low to counteract negative buoyancy. However, because hydrodynamic lift scales with velocity^2, lift production by the fins is less important at higher speeds when lift derived from flows over the body and keeled arms is significant.

Propulsive efficiency

Employing both the jet and fins should improve overall propulsive efficiency because thrust is distributed across multiple propulsors, allowing each propulsor to impart lower fluid velocity than when acting alone. This was true in many sequences when both the fins and jet were active, with overall propulsive efficiency increases of 2–19% when fin contributions were added to jet contributions. These 3D velocimetry results are similar to propulsive efficiency increases of 0.8–10.2% calculated using 2D DPIV data (Bartol et al., 2008). In some sequences, however, fin activity was found to decrease overall propulsive efficiency measurements by as much as 11%. This decrease is consistent with the observed higher propulsive efficiencies for jet-dominated sequences compared with fin-dominated sequences in the present study. The fins sometimes produced significant drag, resulting in high excess kinetic energy relative to thrust production. Although this excess kinetic energy can reduce propulsive efficiency, drag-induced fin motions can also improve stability during steady swimming, aiding the squid in maintaining consistent trajectories, as is the case with the pectoral fins of some fishes (Drucker, 2002, 2003; Drucker and Lauder, 1999).

Propulsive efficiencies in the present study are in reasonable agreement with those of previous studies. The overall mean propulsive efficiency for this study (η=65.5%) is consistent with a DPIV-derived mean propulsive efficiency of 64.0% for *L. brevis* of similar sizes (Bartol et al., 2009b) but is lower than that reported in a more limited *L. brevis* dataset (78%) (Bartol et al., 2008). As was the case in previous studies (Anderson and Grosenbaugh, 2005; Bartol et al., 2009b), propulsive efficiency increased with speed, reaching values as high as 96%. Thus, the propulsive efficiency of jet-based squid at high speeds is not as low as previously assumed (Alexander, 1968; Lighthill, 1975; Vogel, 2003). Furthermore, the finding that jet-dominated sequences have higher propulsive efficiencies than fin-dominated sequences challenges the presumption that fins are more efficient than the jet because they interact with larger volumes of water with each cycle (Bartol et al., 2001b; Hoar et al., 1994; Vogel, 2003).

Based on impulse and kinetic energy measurements derived from 2D vorticity fields, jet mode I was found to have higher propulsive efficiency than jet mode II (Bartol et al., 2008, 2009b). These results were tempered somewhat by the inability to include fin contributions in the DPIV-derived measurements, as these studies focused on jet hydrodynamics. In the present study, contributions from both the fins and jet could be included in propulsive efficiency calculations. Swimming sequences with jets that produced isolated vortex ring wakes had higher propulsive efficiency (η=78.6±7.6%) than sequences with jets producing elongated regions of concentrated vorticity (mean propulsive efficiency=67.9±19.2%). Short pulses with short jet periods (jet mode I) generate impulses with greater proportional impact from over-pressure at the funnel exit plane compared with longer jets (Krueger and Gharib, 2003), which has the potential to improve propulsive efficiency. The observed higher propulsive efficiency for jet mode I relative to jet mode II in the present 3D velocimetry study together with results from 2D velocimetry studies (Bartol et al., 2009b) and mechanical pulsed jet studies (Moslemi and Krueger, 2010; Nichols and Krueger, 2012; Nichols et al., 2008; Whittlesey and Dabiri, 2013) provide strong support for the propulsive benefits of short jet pulses that produce vortex rings.

Swimming direction

Previous studies have described forward and backward swimming in squids (Bartol et al., 2001b, 2009b; Hanlon et al., 1983; Vecchione and Roper, 1991), including detailed kinematic data of *L. brevis* (Bartol et al., 2001b). Clearly, both modes are important ecologically for squids. The tail-first mode is advantageous for steady, high-speed, economical swimming over large distances and for escape jetting (Bartol et al., 2001b; Gosline and DeMont, 1985; O'Dor, 1988), whereas the arms-first mode is important for prey investigation and strikes, low-speed exploration of complex habitats, and antagonistic encounters (Bartol et al., 2001b; Hanlon and Messenger, 1998). When swimming arms-first, squid can observe and respond to potential threats and prey targets ahead, especially when the arms do not obstruct the visual field. Keeping the fins highly active and exhibiting hydrodynamic flexibility, as evident by the fin/jet vortex wake interactions observed in the arms-first orientation here, certainly aids the squid in making rapid course corrections when sensing the environment. Given that tail-first swimming is preferred over arms-first swimming for steady swimming and that funnel curvature requirements are reduced in the tail-first mode, it was thought that tail-first swimming would have a propulsive efficiency advantage. However, no significant difference in propulsive efficiency between the orientations was detected even though tail-first swimming was employed over a wider range of swimming speeds (0–10.0 DML s^{-1}) than arms-first swimming (0–6.6 DML s^{-1}). The lack of difference in propulsive efficiency likely reflects the versatility of the dual-mode system. Certainly, increased fin activity during arms-first swimming can produce an added thrust benefit, as evident by the results of the present study, and this can augment jet thrust to improve overall propulsive efficiency. This added fin thrust may allow for reduced funnel curvature when directing the jet rearward in the arms-first mode, which is supported by higher observed mean jet angles for arms-first swimming (45.0±21.7 deg) versus tail-first swimming (38.4±22.0 deg). Therefore, based on the efficiency results of this study, it appears that coordination between the fins and jet contributes to high propulsive efficiency in both directions.

The jet wakes for arms-first and tail-first swimming differed at high speeds. During arms-first high-speed swimming, highly pulsed short vortex ring jets were consistently produced. While this was also sometimes observed during tail-first swimming, longer jets with ring elements were more common. The reason for this is not entirely clear. One possibility is that refilling is facilitated in the arms-first mode because water can enter directly into the mantle cavity, allowing for high pulsing rates. Although fin activity was not always present during high-speed swimming, it was more frequent during arms-first swimming than during high-speed tail-first swimming. At least for certain sequences, rapidly pulsed jets could be coupled with fin thrust production to produce sufficient overall thrust for high-speed arms-first swimming. Given that shorter, frequent pulses (jet mode I) have the highest propulsive efficiency, this strategy seems reasonable and is a second potential reason for the jet wake differences. A third possibility for the observed differences relates to muscle mechanics. When in the arms-first mode, it is likely difficult for the circular muscles in the funnel, which are antagonists to radial funnel muscles, to maintain optimal aperture control over long jets while the funnel is significantly curved. Aperture regulation during rapid short pulses would certainly be easier to achieve. Further study into the muscle mechanics of funnels would provide useful insight into this prediction.

Conclusions

The present study represents an important step toward understanding multifaceted 3D flows from multi-propulsor systems. The 3D velocimetry technique used here allowed for the study of two hydrodynamically distinct, spatially separated propulsors, a pulsed jet and undulatory/oscillatory fins. The results indicate there is considerable complexity in the wakes of both propulsive systems, with several different patterns of vortex-wake flows being produced, some of which are highly asymmetric. While some flow features are seemingly quite different, e.g. vortex rings versus elongated jets, others are harder to distinguish, e.g. interconnected vortex ring structures. With future application of 3D flow quantitative systems for studying biologically relevant wakes, it will be increasingly important to have quantitative tools for distinguishing relevant features of wake patterns. The development of mathematical tools for quantitative flow pattern categorization is needed to advance the field of biological fluid dynamics in the study of 3D flows.

Acknowledgements

We especially thank Carly York for assistance during animal capture and maintenance, data collection and processing. We also thank the staff at the VIMS ESL for field assistance and TSI, Inc. for providing an additional software key for processing.

Competing interests

The authors declare no competing or financial interests.

Author contributions

I.K.B., P.S.K. and J.T.T. worked together at developing the experimental approach and protocols for this project. I.K.B. and R.A.J. collected the data and performed all analyses. P.S.K. and S.W. developed all Matlab code for this project. All authors provided input on data processing/analysis and all authors played significant roles in the preparation of this manuscript.

Funding

This project was supported by the National Science Foundation (IOS 1115110 to I.K.B., P.S.K. and J.T.T.).

References

Alexander, R. (1968). *Animal Mechanics*. Seattle, WA: University of Washington Press.

Anderson, E. and DeMont, M. E. (2005). The locomotory function of the fins in the squid *Loligo pealei*. *Mar. Freshw. Behav. Physiol.* **38**, 169-189.

Anderson, E. J. and Grosenbaugh, M. (2005). Jet flow in steadily swimming adult squid. *J. Exp. Biol.* **208**, 1125-1146.

Anderson, E. J. and DeMont, M. E. (2000). The mechanics of locomotion in the squid *Loligo pealei*: locomotory function and unsteady hydrodynamics of the jet and intramantle pressure. *J. Exp. Biol.* **203**, 2851-2863.
Bartol, I. K., Mann, R. and Patterson, M. R. (2001a). Aerobic respiratory costs of swimming in the negatively buoyant brief squid *Lolliguncula brevis*. *J. Exp. Biol.* **204**, 3639-3653.
Bartol, I. K., Patterson, M. R. and Mann, R. (2001b). Swimming mechanics and behavior of the shallow-water brief squid *Lolliguncula brevis*. *J. Exp. Biol.* **204**, 3655-3682.
Bartol, I. K., Krueger, P. S., Thompson, J. T. and Stewart, W. J. (2008). Swimming dynamics and propulsive efficiency of squids throughout ontogeny. *Integr. Comp. Biol.* **48**, 720-733.
Bartol, I. K., Krueger, P. S., Stewart, W. J. and Thompson, J. T. (2009a). Pulsed jet dynamics of squid hatchlings at intermediate Reynolds numbers. *J. Exp. Biol.* **212**, 1506-1518.
Bartol, I. K., Krueger, P. S., Stewart, W. J. and Thompson, J. T. (2009b). Hydrodynamics of pulsed jetting in juvenile and adult brief squid *Lolliguncula brevis*: evidence of multiple jet 'modes' and their implications for propulsive efficiency. *J. Exp. Biol.* **212**, 1889-1903.
Burgmann, S., Brücker, C. and Schröder, W. (2006). Scanning PIV measurements of a laminar separation bubble. *Exp. Fluids* **41**, 319-326.
Couch, L. D. and Krueger, P. S. (2011). Experimental investigation of vortex rings impinging on inclined surfaces. *Exp. Fluids* **51**, 1123-1138.
Dabiri, J. O. and Gharib, M. (2005b). The role of optimal vortex formation in biological fluid transport. *Proc. R. Soc. B Biol. Sci.* **272**, 1557-1560.
Drucker, E. G. (2002). Experimental hydrodynamics of fish locomotion: functional insights from wake visualization. *Integr. Comp. Biol.* **42**, 243-257.
Drucker, E. G. (2003). Function of pectoral fins in rainbow trout: behavioral repertoire and hydrodynamic forces. *J. Exp. Biol.* **206**, 813-826.
Drucker, E. and Lauder, G. (1999). Locomotor forces on a swimming fish: three-dimensional vortex wake dynamics quantified using digital particle image velocimetry. *J. Exp. Biol.* **202**, 2393-2412.
Fish, F. E. (2002). Balancing requirements for stability and maneuverability in cetaceans. *Integr. Comp. Biol.* **42**, 85-93.
Flammang, B. E., Lauder, G. V., Troolin, D. R. and Strand, T. E. (2011a). Volumetric imaging of fish locomotion. *Biol. Lett.* **7**, 695-698.
Flammang, B. E., Lauder, G. V., Troolin, D. R. and Strand, T. (2011b). Volumetric imaging of shark tail hydrodynamics reveals a three-dimensional dual-ring vortex wake structure. *Proc. R. Soc. B Biol. Sci.* **278**, 3670-3678.
Foyle, T. P. and O'Dor, R. K. (1988). Predatory strategies of squid (*Illex illecebrosus)* attacking small and large fish. *Mar. Behav. Physiol.* **13**, 155-168.
Gharib, M., Pereira, F., Dabiri, D., Hove, J. R. and Modarress, D. (2002). Quantitative flow visualization: toward a comprehensive flow diagnostic tool. *Integr. Comp. Biol.* **42**, 964-970.
Gosline, J. and DeMont, M. (1985). Jet-propelled swimming in squids. *Sci. Am.* **252**, 96-103.
Gosline, J. M. and Shadwick, R. E. (1983). The role of elastic energy storage mechanisms in swimming: an analysis of mantle elasticity in escape jetting in the squid, *Loligo Opalescens*. *Can. J. Zool.* **61**, 1421-1431.
Gosline, J. M., Shadwick, R. E. and DeMont, M. E. (1983). Elastic energy storage and power output in squid mantle muscle. *J. Biomech.* **16**, 293.
Graff, E. C. and Gharib, M. (2008). Performance prediction of point-based three-dimensional volumetric measurement systems. *Meas. Sci. Technol.* **19**, 075403.
Hanlon, R. T. and Messenger, J. B. (1998). *Cephalopod Behaviour*. Cambridge: Cambridge University Press.
Hanlon, R. T., Hixon, R. F. and Hulet, W. H. (1983). Survival, growth, and behavior of the loliginid squids *Loligo plei*, *Loligo pealei*, and *Lolliguncula brevis* (Mollusca: Cephalopoda) in closed sea water systems. *Biol. Bull.* **165**, 637-685.
Hoar, J. A., Sim, E., Webber, D. M. and O'Dor, R. K. (1994). The role of fins in the competition between squid and fish. In *Mechanics and Physiology of Animal Swimming* (ed. L. Maddock, Q. Bone and J. M. V. Rayner), pp. 27-33. Cambridge: Cambridge University Press.
Jastrebsky, R. A., Bartol, I. K. and Krueger, P. S. (2016). Turning performance in squid and cuttlefish: unique dual mode, muscular hydrostatic systems. *J. Exp. Biol*. In press
Johnsen, S. and Kier, W. M. (1993). Intramuscular crossed connective tissue fibres: skeletal support in the lateral fins of squid and cuttlefish (Mollusca: Cephalopoda). *J. Zool.* **231**, 311-338.
Johnson, W., Soden, P. D. and Trueman, E. R. (1972). A study in jet propulsion: an analysis of the motion of the squid, *Loligo Vulgaris*. *J. Exp. Biol.* **56**, 155-165.
Kajitani, L. and Dabiri, D. (2005). A full three-dimensional characterization of defocusing digital particle image velocimetry. *Meas. Sci. Technol.* **16**, 790-804.
Kier, W. M. (1988). The arrangement and function of molluscan muscle. In *The Mollusca, Form and Function*, Vol. 11 (ed. E. R. Trueman and M. R. Clarke), pp. 211-252. New York: Academic Press.
Kier, W. M. (1989). The fin musculature of cuttlefish and squid (Mollusca, Cephalopoda): morphology and mechanics. *J. Zool.* **217**, 23-38.
Kier, W. and Leeuwen, J. (1997). A kinematic analysis of tentacle extension in the squid *Loligo pealei*. *J. Exp. Biol.* **200**, 41-53.
Kier, W. M. and Smith, K. K. (1985a). Tongues, tentacles and trunks: the biomechanics of movement in muscular-hydrostats. *Zool. J. Linn. Soc.* **83**, 307-324.
Kier, W. M. and Smith, K. K. (1985b). Tongues, tentacles and trunks. *J. Linn. Soc. Lond. Zool.* **83**, 23-38.
Kier, W. M. and Thompson, J. T. (2003). Muscle arrangement, function and specialization in recent coleoids. *Berl. Palaobiol. Abh.* **3**, 141-162.
Krueger, P. S. and Gharib, M. (2003). The significance of vortex ring formation to the impulse and thrust of a starting jet. *Phys. Fluids* **15**, 1271-1281.
Krueger, P. S. and Gharib, M. (2005). Thrust augmentation and vortex ring evolution in a fully-pulsed jet. *AIAA J.* **43**, 792-801.
Lighthill, M. (1975). *Mathematical Biofluidynamics*. Philadelphia, PA: Society for Industrial and Applied Mathematics.
Messenger, J. B. (1968). The visual attack of the cuttlefish, *Sepia officinalis*. *Anim. Behav.* **16**, 342-357.
Moslemi, A. A. and Krueger, P. S. (2010). Propulsive efficiency of a biomorphic pulsed-jet underwater vehicle. *Bioinspir. Biomim.* **5**, 036003.
Munson, B. R., Young, D. F., Okiishi, T. H. Huebsch, W. W. (2009). *Fundamentals of Fluid Mechanics*, 6th edn. Hoboken, NJ: John Wiley & Sons, Inc.
Nauen, J. C. and Lauder, G. V. (2002). Quantification of the wake of rainbow trout (*Oncorhynchus mykiss*) using three-dimensional stereoscopic digital particle image velocimetry. *J. Exp. Biol.* **205**, 3271-3279.
Nichols, J. T. and Krueger, P. S. (2012). Effect of vehicle configuration on the performance of a submersible pulsed-jet vehicle at intermediate Reynolds number. *Bioinspir. Biomim.* **7**, 036010.
Nichols, J., Moslemi, A. and Krueger, P. S. (2008). Performance of a self-propelled pulsed-jet vehicle. 38th AIAA Fluid Dynamics Conference, Seattle, WA (AIAA-2008-3720).
O'Dor, R. K. (1988). The forces acting on swimming squid. *J. Exp. Biol.* **442**, 421-442.
O'Dor, R. K. and Webber, D. M. (1991). Invertebrate athletes: trade-offs between transport efficiency and power density in cephalopod evolution. *J. Exp. Biol.* **160**, 93-112.
Pereira, F. and Gharib, M. (2002). Defocusing digital particle image velocimetry and the three-dimensional characterization of two-phase flows. *Meas. Sci. Technol.* **13**, 683-694.
Pereira, F. and Gharib, M. (2004). A method for three-dimensional particle sizing in two-phase flows. *Meas. Sci. Technol.* **15**, 2029-2038.
Pereira, F., Gharib, M., Dabiri, D. and Modarress, D. (2000). Defocusing digital particle image velocimetry: a 3-component 3-dimensional DPIV measurement technique. Application to bubbly flows. *Exp. Fluids* **29**, S078-S084.
Pereira, F., Stüer, H., Graff, E. C. and Gharib, M. (2006). Two-frame 3D particle tracking. *Meas. Sci. Technol.* **17**, 1680-1692.
Saffman, P. G. (1992). *Vortex Dynamics*. Cambridge: Cambridge University Press.
Standen, E. M. and Lauder, G. V. (2007). Hydrodynamic function of dorsal and anal fins in brook trout (*Salvelinus fontinalis*). *J. Exp. Biol.* **210**, 325-339.
Stewart, W. J., Bartol, I. K. and Krueger, P. S. (2010). Hydrodynamic fin function of brief squid, *Lolliguncula brevis*. *J. Exp. Biol.* **213**, 2009-2024.
Troolin, D. R. and Longmire, E. K. (2010). Volumetric velocity measurements of vortex rings from inclined exits. *Exp. Fluids* **48**, 409-420.
Vecchione, M. and Roper, C. (1991). Cephalopods observed from submersibles in the western North Atlantic. *Bull. Mar. Sci.* **49**, 433-445.
Vogel, S. (1987). Flow-assisted mantle cavity refilling in jetting squid. *Biol. Bull.* **172**, 61-68.
Vogel, S. (2003). *Comparative Biomechanics: Life's Physical World*. Princeton, NJ: Princeton University Press.
Webb, P. W. (2002). Control of posture, depth, and swimming trajectories of fishes. *Integr. Comp. Biol.* **42**, 94-101.
Webber, D. M. and O'Dor, R. K. (1986). Monitoring the metabolic rate and activity of free-swimming squid with telemetered jet pressure. *J. Exp. Biol.* **126**, 205-224.
Weihs, D. (1977). Periodic jet propulsion of aquatic creatures. *Fortschritte Zool.* **24**, 171-175.
Weihs, D. (2002). Stability versus maneuverability in aquatic locomotion. *Integr. Comp. Biol.* **42**, 127-134.
Whittlesey, R. and Dabiri, J. (2013). Optimal vortex formation in a self-propelled vehicle. *J. Fluid Mech.* **737**, 78-104.